

Evaluation of Geomagnetic Field Models using Magnetometer Measurements for Satellite Attitude Determination System at Low Earth Orbits: Case Studies

Demet Cilden-Guler¹, Zerefsan Kaymaz, and Chingiz Hajiyev

Istanbul Technical University, Faculty of Aeronautics and Astronautics, Maslak, Istanbul, Turkey

Abstract

In this study, different geomagnetic field models are compared in order to study the errors resulting from the representation of magnetic fields that affect the satellite attitude system. For this purpose, we used magnetometer data from two Low Earth Orbit (LEO) spacecraft and the geomagnetic models IGRF-12 (Thébault et al., 2015) and T89 (Tsyganenko, 1989) models to study the differences between the magnetic field components, strength and the angle between the predicted and observed vector magnetic fields. The comparisons were made during geomagnetically active and quiet days to see the effects of the geomagnetic storms and sub-storms on the predicted and observed magnetic fields and angles. The angles, in turn, are used to estimate the spacecraft attitude and hence, the differences between model and observations as well as between two models become important to determine and reduce the errors associated with the models under different space environment conditions. We show that the models differ from the observations even during the geomagnetically quiet times but the associated errors during the geomagnetically active times increase. We find that the T89 model gives closer predictions to the observations, especially during active times and the errors are smaller compared to the IGRF-12 model. The magnitude of the error in the angle under both environmental conditions was found to be less than 1°. For the first time, the geomagnetic models were used to address the effects of the near Earth space environment on the satellite attitude.

Key Words: Spacecraft attitude, IGRF-12, T89 model, geomagnetic storms

1. Introduction

Magnetometers are one of the attitude determination sensors for small satellites at Low Earth Orbit (LEO). In the absence of the actual and reliable magnetic field measurements, on-board model magnetometers and a model of the Earth's magnetic field are needed for the prediction of the geomagnetic field at the satellite's altitude. The conventional methodology while estimating the satellite's attitude involves the angle between the magnetic field vectors from the simulated magnetometer and the model of the Earth's geomagnetic field. Therefore, the accuracy of the geomagnetic fields from the model is critical for a precise attitude determination. As scientific payloads, the magnetometers on-board the satellites return data in space within their built-in

¹ Corresponding Author, cilden@itu.edu.tr

precision and are placed one or two meters away from the spacecraft body on a boom in order to avoid from the magnetic effects created by the satellite itself and its nearby surrounding environment. Simulated magnetometers, on the other hand, use the magnetic field direction from a geomagnetic field model, most widely IGRF (Thébault et al., 2015), to determine the parameters of the satellite attitude. Both magnetometers include several errors and bias sources that will affect the satellite's attitude. Current state-of-the-art satellite magnetometers are highly improved both in accuracy, and precision and resolution as well as in physical size. Among several satellite magnetometers, two of the most often used ones are the Flux Gate Magnetometers (FGM) and Search Coil Magnetometers (SCM) that use tri-axial configuration. Many of the bias and random errors may be reduced or prevented prior to the launch during the ground tests or on orbit after the launch with having an additional sensor for calibration on the satellite. There are several methods proposed in the literature for magnetometer calibration without attitude information. The most-commonly known method is TWOSTEP algorithm that, after the centering approximation, uses a second step employing the centered estimation, found by an approximation, as an initial value to an iterative Gauss-Newton method that avoids divergence problems as other algorithms cannot (R Alonso and Shuster, 2002; R. Alonso and Shuster, 2002). In parallel to the advancing technologies in space industry, providing that the errors that may be resulted from real magnetometer sensors on board are negligible to affect the attitude, the source of the most of the errors then would be associated with the environmental conditions in case of the real magnetometers and from the bias, noise and scaling factors in case of the simulated magnetometers and how they are handled during onboard processing in space.

The errors in attitude determination are determined in the literature using different approaches. An approach that was suggested by (Inamori and Nakasuka, 2012) is to compare the magnetometer measurements with the magnetic fields predicted by the IGRF geomagnetic model and aims to remove the bias and scaling errors. In this case, IGRF predictions are used to calibrate and optimize the simulated magnetometer magnetic fields (Archer et al., 2015; Inamori and Nakasuka, 2012). The other approach involves the conversion of the IGRF model magnetic field to the satellite body coordinates. In these studies, IGRF model is assumed to represent the geomagnetic field correctly. These studies imply that a good representation of the geomagnetic field is an essential part of the attitude determination process and the closer the geomagnetic model results to the real geomagnetic fields in space at the satellite's altitude, the more accurate the satellite attitude.

For the determination of the satellite's attitude angles, Extended Kalman Filter (EKF), Unscented Kalman Filter (UKF) and similar filters or single-frame methods such as q, QUEST, SVD etc. are widely used (Ainscough et al., 2015; Hajiyev and Bahar, 2003; Hajiyev and Cilden Guler, 2017; Vinther et al., 2011). The source of the error in the determination of the attitude angles may come from the model magnetometer calibrated using IGRF predictions at the satellite altitude. Some of the inaccuracies related to the geomagnetic model, IGRF, used by the model magnetometer result from the model assumptions, the insufficient experimental data, or both. For epoch 2000, the coefficients are provided to degree and order 13 and 0.1 nT precision for IGRF-12 model (Thébault et al., 2015). In this study, we investigate the effects of the LEO orbit environmental conditions on the satellite attitude system, which are superimposed on the Earth's

geomagnetic field as a result of magnetospheric substorms. As these effects are not taken into account in IGRF, the magnetic field at the satellite altitude during these times is underestimated by the simulated magnetometer. Some of the specific questions that we address are:

- 1- How well does the magnetic field (magnitude and direction) estimated by the geomagnetic field model accurately represent the real geomagnetic field at LEO altitudes,
- 2- How much the Earth's geomagnetic field varies during the magnetic storms and substorms at LEO altitudes? Consequently, how much these variations affect the predictions of geomagnetic models, e.g. IGRF?
- 3- What is the error that these will create on the spacecraft attitude as referred from the angle between the measured magnetic field and the field from the geomagnetic model?
- 4- Which geomagnetic field model gives closer estimates to the measured magnetic field at the satellite altitude at LEO? i.e. determine and compare the performance of different models.

In the following sections, we first describe the data sets and the methodology used in this study and then present the results and discussion. In the last section, we give a summary and conclusions.

2. Data and Methodology

The first and the second questions given above are investigated by looking at the differences between the magnetic field vector measurements obtained from a real magnetometer placed on a LEO orbiting satellite and a chosen geomagnetic model during the geomagnetically active and quiet times. As for LEO orbiting satellites, we selected C/NOFS, and SWARM satellite magnetic field measurements. The data from these spacecraft were obtained from (“Coordinated Data Analysis Web (CDAWeb),” 2017), and (“Swarm Data Access - FTP,” 2017). Both satellites use a fluxgate magnetometer placed on a boom away from the satellite. Regarding the geomagnetic field model of the Earth, in recent years, there have been several new geomagnetic models developed to represent the geomagnetic field under different external conditions such as Tsyganenko models (Farfield, 1991; Peredo et al., 1993; Tsyganenko, 2008, 1995, 1989), CHAOS (Finlay et al., 2016; Olsen et al., 2006), POMMES-6 (Maus et al., 2010) etc. in addition to the IGRF model. In this study, we used 1989 version of Tsyganenko magnetospheric model (T89) and the last version of the IGRF model (IGRF-12) to study the geomagnetic field of the Earth at LEO altitudes. The satellite attitude has been studied based on the angle between the magnetic field vectors measured on the satellite and from the model on orbit. Difference in the components of the magnetic field vectors is mostly used as a unit vector. Therefore, the angle between the magnetic field of the modeled and measured field affects the degree of accuracy in the satellite’s attitude. In this study, it is our interest to evaluate these models by comparing their predictions with the magnetometer measurements from the selected satellites given above. For attitude determination system, IGRF model is most commonly used model. However, the difference between the magnetic fields of the sensor and model increases when the geomagnetic activity occurs. Hence, several models that take into account the external variations resulting from the solar wind and interplanetary magnetic field superimposed on the Earth’s geomagnetic field are of great importance in determination of the satellite’s attitude correctly.

2.1. Geomagnetic Models

The simplest model of Earth's geomagnetic field is the dipole field approximation. However, the dipole approximation fails to represent the geomagnetic field at distances far away from the Earth owing to the modifications of the geomagnetic field lines by the solar wind. As a result, the magnetometers are not reliable to be used as attitude sensors at farther distances from the Earth. In International Geomagnetic Reference Field (IGRF) models, Earth's main magnetic field is described by the series of spherical harmonic coefficients that describe the secular variation of the Earth's magnetic field. Earth's magnetic field in IGRF-12 model with order of 13th is expressed as the gradient of a scalar potential function. In most of the nanosatellite missions, truncated versions as 7th to 10th order of IGRF are preferred and this might cause a reduced accuracy on the model outputs (Lowes, 2014). IGRF-12 is a model using several candidate models which are based on different groups of datasets and time intervals from the Swarm, CHAMP, Ørsted, SAC-C missions (Thébault et al., 2015). The accuracy of the IGRF-10 and IGRF-11 models were found to be accurate within 1° for 92% times in the upper atmosphere (Matteo and Morton, 2011). Based on long term satellite observations, these models represent the average geomagnetic conditions and neglect the variations resulting from the geomagnetic disturbances superimposed on the main geomagnetic field at the satellites altitudes. During the geomagnetic storms and sub-storms, Earth's main magnetic field undergo several variations. These variations are treated as noise or error and cannot be fully represented in the attitude determination most of the time. The magnetic field strength and the direction change in time scale from seconds to hours and from a few nanoTeslas (nT) to orders of 1000s of nT depending on the altitude of the satellite. For example, in the geostationary orbit, the magnitude of the perturbations can be as large as on the orders of 200nT. Additionally, these phenomena occur several times in a week during the high solar activity periods while one or two occur during the low solar activity period. Therefore, the geomagnetic storms and substorms can have an appreciable effect on the satellite's attitude estimated by the IGRF model and subsequently the simulated magnetometer.

T89 model (1989) is an empirical model of the magnetosphere based on large satellite data from the low altitudes of the Earth to large distances in the magnetotail and in the solar wind. Therefore, it covers a large spectrum of magnetospheric and solar wind conditions in addition to upper atmospheric conditions at LEO altitudes. The model uses IGRF as a base model of the geomagnetic field close to Earth but includes the external effects inherited in the data from several magnetospheric and solar wind satellites such as IMP, HEOS, ISEE spacecraft etc. (Peredo et al., 1993; Tsyganenko, 1989). So that in addition to the main field (internal) given by IGRF (B_{INT}), it includes extraterrestrial effects (B_{EXT}). The magnetic field in space can be represented by adding these components (Tsyganenko, 1989):

$$B_{TOT} = B_{INT} + B_{EXT} \quad (1)$$

where,

$$B_{EXT} = B_{RC} + B_{MP} + B_{Region1-2} + B_T \quad (2)$$

As seen in (2), more explicitly, B_{EXT} includes effects from Ring current (B_{RC}), tail current (B_T), magnetopause currents (B_{MP}) and Region 1 and 2 currents ($B_{Region1-2}$). Data sets are categorized with respect to the geomagnetic activity index K_p which represents the geomagnetically active or quiet times for external sources. Hence, the inputs for the T89 model are K_p , the position of the satellite, and time of the year to generate external magnetic field effects at the satellite's altitude. Improved versions are available that includes several other external sources that affect the total magnetic field. For example, the T05 source code is described for dynamical empirical model of the inner storm-time magnetosphere, while T89 is a magnetic field model with warped tail current sheet. We use T89 version to determine the extraterrestrial effects on the magnetic field which can affect the attitude accuracy of small satellites. Since T89 model uses IGRF model for internal sources near the Earth, at LEO orbits altitudes, both models are expected to give similar results if there are no extraterrestrial effects. Earth's dipole field should dominate as we close to the Earth over the extraterrestrial sources. However, during the geomagnetically active times, differences from the dipole model arise due to the currents flowing from the magnetosphere into the Earth's atmosphere. Following sections present our preliminary results from the model-to-observation comparisons as well as the model-to-model comparisons and discuss their implications from the satellite attitude perspective. The sketch in Figure 1 outlines the procedures we apply for the model-model and model-observation comparisons.

2.2. Coordinate Systems

When dealing with the Earth's geomagnetic field, it is unavoidable to work with different coordinate systems depending on the type of the problem. Figure 2 illustrates the coordinates systems involved in this study at the location of the satellite in space. The satellite magnetometer data are available mostly in ECEF (Earth Centered, Earth Fixed). In ECEF system, the z-axis is along the spin axis of the Earth and pointing to the north pole. The x-axis points towards the intersection of the 0° latitude (i.e. the equator) and 0° longitude and y-axis completes the right-handed coordinate system, passing through 0° latitude (i.e. the equator) and 90° longitude. Cartesian coordinates that the ECEF was represented as in the GEO (Geographic Coordinates) frame was also shown in Figure 2. In the figure, ENU indicates the East, North, and Up respectively.

As indicated in the sketch in Figure 1, throughout this study, we used MAG (Geomagnetic) coordinates for comparisons between the magnetic field vectors from the satellite magnetometer and the geomagnetic models. Both the model magnetic field and the satellite magnetic field data were obtained in this coordinate system. In MAG system, z-axis aligns with the dipole axis and y-axis is perpendicular to the plane containing the dipole axis and the rotation axis of the Earth. The x-axis completes the right-handed system (Russel, 1971). For near Earth space regions, such as LEO, where the Earth's magnetic field dominates, the magnetic fields are best represented in MAG system (Hapgood, 1992; Russel, 1971).

Body and orbit reference frames are the main coordinate systems for attitude determination system. The body frame of reference describes the vectors in a coordinate system centered at the center of mass of the satellite. Orbital coordinate system, on the other hand, refers to the coordinate

system when the satellite is in its orbit. Attitude angles are found using a transformation matrix from the orbital reference system to body coordinate system. Satellite motion in each direction on orbit is described by the Euler angles (roll, pitch, yaw about x, y, z axes respectively) which can be determined in the filter by using the geomagnetic field direction at the location of the satellite.

2.3 Satellite Observations

Verification of the magnetic field models can be achieved by using observations from a reliable magnetometer such as fluxgate. In this study, C/NOFS, and SWARM satellites, which carry on-board fluxgate magnetometers, at LEO orbits were used for comparisons with the results from the geomagnetic field models and for determination of the attitude angles. Orbital and instrumental characteristics of these satellites were presented in Table-1. (“Communications/Navigation Outage Forecasting System (C/NOFS),” 2016; European Space Agency, 2016). C/NOFS (Communication/Navigation Outage Forecast System) is a US mini-satellite launched on April 16, 2008 and ended in November 22, 2015 (Krebs, 2016). It was designed to forecast the ionospheric irregularities in Earth’s equatorial region. The spacecraft has an elliptical orbit with low inclination at altitudes varying from 405 to 853 km and an attitude better than 0.1° using the star sensors (Pfaff et al., 2010). The accuracy of the magnetic field instrument on C/NOFS has the accuracy of 0.1 nT (Pfaff, n.d.). Additionally, the spacecraft was listed in having one of the most precise GPS receivers flown in space as between 1-45 cm accuracy (Lichten, 2008). SWARM (Geomagnetic LEO Constellation) is a mini-satellite constellation mission with 3 satellites, (SWARM A (Alpha, SWARM B (Bravo) and SWARM C (Charlie), built by ESA. The constellation was launched in Nov. 22, 2013 and is still in operation. SWARM A and C satellites both have an altitude around 400 km (<450 km) with an inclination of 87.4° . SWARM B (Bravo) has higher altitude around 500 km (<530 km) with 88° inclination. The scientific mission of SWARM constellation pair is to measure and study the magnetic variations of the Earth’s geomagnetic field resulting from the Earth’s core, mantle, crust and oceans, as well as from the ionosphere and magnetosphere; to study the Sun’s influence on Earth system; to understand the impact of solar wind on dynamics of the upper atmosphere. In this study, the magnetic field data from SWARM A satellite were used in our comparisons. The spacecraft carry a magnetic field instrument with an accuracy under 0.5 nT, and has a precise orbit determination under 10 cm (rms) in addition to 3-dimensional position measurements better than 20 m (3σ) and absolute accuracy under 1 arcsec for attitude knowledge (European Space Agency, 2016). In addition, both the magnetic field and position data from both spacecraft were obtained from the institutes’ public web sites, which in the case of C/NOFS, it is NASA’s CDWeb (<http://cdaweb.gsfc.nasa.gov>) and in the case of SWARM, it is ESA’s web-site (<http://earth.esa.int/>). Both data sets from both spacecraft were provided in 1 sec resolution. As C/NOFS’s apogee is larger than that of SWARM A, it is expected that the extraterrestrial effects will be more dominant especially when the satellite is moving towards its apogee at higher altitudes. Higher altitudes are more susceptible to the effects originated from the Earth’s magnetosphere and outside. Therefore, the altitude of the satellite is important in determining the degree of the geomagnetic storm effects.

3. Analysis and Results

As our purpose of study is threefold, namely, one is to compare the geomagnetic field models with satellite observations at LEO orbits; two is to determine which model approximates the observations better; and three is to determine the effects of differences between the models and observations on the attitude angles by evaluating the angle between magnetic field orientations of the model and observations. These comparisons were made during the magnetically disturbed days to reveal the effects of the magnetic storms and magnetospheric sub-storms on the geomagnetic field at LEO and on the attitude angles. For the comparisons between the models and the observations, first we looked for the time intervals when there are geomagnetic storms occurred in the magnetosphere and both the magnetic field and the position data from the satellites exist during that time interval. Taking the operation times of these satellites given in Table 1 into account, we have selected 3 different magnetically quiet days when there are no geomagnetic storms or magnetospheric substorms in the magnetosphere and 3 different magnetically disturbed days, i.e. when there are magnetic storms and substorms in the magnetosphere at various levels from weak to strong. Table 2 presents these cases to be studied in detail in the following sections.

Quiet or disturbed days were chosen by looking at the geomagnetic indices, K_p , D_{st} and AE (Data Analysis Center for Geomagnetism and Space Magnetism, n.d.). These are the magnetic indices that show the level of extraterrestrial disturbances resulting from the interaction between the solar wind and Earth's magnetosphere. They are calculated based on the geomagnetic field measured on the ground magnetic observatories. D_{st} index refers to the Disturbance Storm Time index and conveniently shows the presence of the geomagnetic storms initiated when the solar wind first hits the Earth's magnetosphere on the dayside at the subsolar point. This compression depending on the strength of the solar wind dynamic pressure is detected in D_{st} index as a positive excursion from the quiet time level of D_{st} which is known as the sudden commencement. During a typical geomagnetic storm, the sudden commencement starts at 20 nT. This is followed by a large drop in the geomagnetic field, which defines the geomagnetic storm main phase. D_{st} index is obtained from geomagnetic observatories located at the low latitudes around 20° of the equator. It is a good indicator of the ring current in the geomagnetic tail that increases as a result of increased tail currents during the geomagnetic storms following the initial compression on the dayside. Geomagnetic activity that causes D_{st} to drop below -40 nT are considered as a geomagnetic storm (Gonzalez et al., 1994). The more negative the D_{st} index, the stronger the geomagnetic activity is. Auroral Electrojet index (AE) index, on the hand, gives the geomagnetic disturbances measured at the high latitudes resulting from the particles coming from the geomagnetic tail as a consequence of the magnetospheric substorms that create the auroral lights over the northern and southern high latitudes. These particles give rise to strong electrical currents at high altitudes in the atmosphere which are known as Auroral Electrojet currents and measured by AE index. The magnetospheric substorms that result in AE index to be larger than 100 nT are considered as magnetospheric substorm. K_p (planetarische Kennziffer) index is the planetary index that shows the global geomagnetic activity level and measured using the magnetic field data from the mid latitude geomagnetic stations. A geomagnetic disturbance with K_p larger than 4 is considered as a storm. Table-3 indicates the level of the geomagnetic storm or substorm depending on the scale of these indices.

Figure 3 presents an example of the magnetic field data measured on-board C/NOFS satellite during the magnetically quiet day, March 7 2009. It presents the magnetic field components in MAG coordinates, i.e. B_x in the north-south direction, B_y in the east-west direction, and B_z as the component in the z-direction which is parallel to Earth's dipole moment, for a stretch of one day from 00:00 UT to 24:00 UT. The periodic variations seen in this figure are due to the orbital motion of the satellite. In order to make comparisons, the differences resulting from the orbital motion were removed by taking the period-averaged magnetic field data. The C/NOFS has an orbital period of 97.3 min (see Table 1). Therefore, a running mean procedure with a window length of 97.3 min (~1.5 hr) were applied on the magnetic field data in this case. This process eliminates the temporal variations less than 1.5 hr as well as the latitudinal variations resulting from the orbit. For the purposes of our study, we think that this procedure is appropriate. In this figure, the black and blue lines give the magnetic field data and the period-averaged magnetic field data. As seen clearly, the running mean process removes the orbital periodicity. Still a slight periodicity that the running mean did not completely removed appears, however this will not affect our comparisons.

Figure 4 represents the first case from C/NOFS satellite. The panels on the left in Figure 4 give the model-data comparisons for a quiet day recorded on March 7, 2009. The panels from top to bottom are K_p index (a), the differences between the magnetic field components measured by on-board magnetometer on C/NOFS satellite and the magnetic field predictions of the models, IGRF (b) and T89 (c), and the differences between two models (d). The blue, red and black colors indicate differences in B_x , B_y , and B_z components. K_p index in panel (a) indicates that the level of geomagnetic activity is low. In fact, for this day, there aren't any geomagnetic activity, thus $K_p = 0$. The line at $K_p = 4$ indicates the threshold after which the day is considered as disturbed. For direct comparisons with the observed magnetic field, the same orbit-averaged running mean procedure was applied on the model magnetic field components as well. The figure was constructed by simply subtracting the magnetic field components of the magnetic field measured on the satellite from those predicted by the models. Therefore, the panels compare the differences between the observed and geomagnetic model predicted magnetic field components. As a result, positive differences in these panels indicate that the model magnetic field is larger than the observed magnetic field while negative differences imply that the observed fields are larger than those of models. Even during this magnetically quiet day, namely in the absence of geomagnetic storms, the model magnetic fields are seen to be quite different than those observed. The largest differences in panels b and c were seen in B_x component, the north-south component of the magnetic field, and the least difference was found in B_z component. Both models overestimate the observed B_x component while on the average they under estimate the B_y component. Both models, on the average, gives slightly larger B_z component than the observed one. Although the differences are small for B_z component, T89 model gives positive differences meaning that the model slightly overestimates B_z component while IGRF shows negative differences indicating the underestimation of the observed B_z . The differences were calculated as the maximum deviations of the models from the observations and any distribution was not assumed for the data. The differences between the models and the observations vary up to +60 nT for B_x component and between 0 and -30 nT for B_y . The difference for B_z component ranges from 0 to 20 nT in T89 and 0 to -20 nT in IGRF. Panel (d) displays the differences between IGRF and T89 models. In this

case, T89 model results were subtracted from those of IGRF model. Both \mathbf{B}_x and \mathbf{B}_y are very close to each other within less than 5 nT but two models differ the most in \mathbf{B}_z component and the difference is seen to be about -20 nT on the average. This implies larger estimates from T89 compared to IGRF for \mathbf{B}_z component. While the model-to-observed magnetic field comparison shows that the models differ the most in \mathbf{B}_x component, model-to-model comparisons indicate the models differ from each other the most in estimating the \mathbf{B}_z component. As for total magnetic field, there are no differences between the model predictions so that the difference is close to zero but both model show a difference from the observations on the order of 50 nT (not shown, Table 4).

The panels on the right in Figure 4 gives a similar comparison during a magnetically active day on March 17, 2013. The panels from top to bottom are the same as in panels on the left in Figure 4. In the first panel, we see that K_p index is larger than 4 from 06:00 UT until the end of the day, with a maximum of 7+ from 06:00 UT to 10:00 UT and from 18:00 UT to 21:00 UT. Average K_p for the day is about 5+. Both panels b and c show that the models give the largest differences from the observations when the geomagnetic activity started at 06:00 UT. The geomagnetic activity stays high from 06:00 UT to 21:00 UT and we see that both IGRF and T89 models differ the most from the observations during this time interval. We can see that the differences in \mathbf{B}_x component before the geomagnetic activity is around 80 nT and increases slowly up to 130 nT after the geomagnetic storm starts and continues to increase to 205 nT till the end of the time scale given in this figure. Differences in both \mathbf{B}_y and \mathbf{B}_z are very close to zero before the geomagnetic storm, but increases after. Differences with the observations in \mathbf{B}_y component in both models vary around -80 nT. However, \mathbf{B}_z component shows differences on the order of 30 to 40 nT in T89 model, while it is around -40 nT in IGRF12 model. Both panels show that \mathbf{B}_x component was overestimated and by component was underestimated in both models. \mathbf{B}_z component, on the other hand, was overestimated in T89 while it is underestimated in IGRF. These comparisons are qualitatively the same as obtained in quiet time case. However, quantitatively, compared to the same panels of quiet day given in Figure 4, the differences between both models and the observations are larger during the magnetically active day by about a factor of 3. Panel d, similar to quiet day case, indicates that the models differ mostly in \mathbf{B}_z component up to 100 nT during the geomagnetic storm interval while the differences between predicted \mathbf{B}_x and \mathbf{B}_y components are small, being on the order of 10 nT before the geomagnetic storm. We see that T89 model gives larger prediction of \mathbf{B}_z component than IGRF. Although not given in these plots, both model exhibit differences with the observations around 200 nT for the total magnetic field during the geomagnetic storm interval while smaller, around 50 nT on average before the storm. Despite this difference with the observations, there are no discernable differences between the predictions of the total magnetic field from both models during the quiet and active day.

Figure 5 compares the angle (α) between the observed and model (T89 and IGRF) magnetic field vectors measured during the quiet (left) and active (right) day using C/NOFS data. The angle was calculated by taking scalar product of two unit vectors. While the first two panels give the level of geomagnetic activity as seen in D_{st} index for geomagnetic storm and AE index for the auroral substorm, the third panel presents the angle calculated. Although D_{st} index variation is small during the active day, AE index is larger than 100 nT indicating the presence of a

magnetospheric substorm in the geomagnetic tail that results in aurora in the ionospheric altitudes. The differences between the quiet and active day angles as well as between the model predictions are clearly demonstrated in these panels. During the quiet day, both models indicate that the angle between predicted and observed vary around 0.15° in panel d on the left. In panel d on the right, T89 predicts smaller angles compared to IGRF model. T89 prediction of the angles stays around 0.12° during the storm day while the angles predicted by IGRF increase after the storm starting at 06:00 UT. This indicates that the magnetic field vector predictions from T89 model are closer to the observations. It is clear that larger differences with the observations during the active days are caused by the geomagnetic storms.

For small satellites, both magnetometer data and a magnetic field model are necessary for the attitude estimations. For most of the cases, the model predicted and measured magnetic field components are used as unit vectors. Therefore, the angle between the model and the observed magnetic field is a key parameter in determining the attitude angles, namely yaw, pitch, and roll. The closer the model predictions to the observed fields, the more accurate the attitude estimates will be. In Figure 5, we see that the angles calculated for both magnetically quiet and active day are small to cause a serious effect on the satellite's attitude. For most small satellite applications, an accuracy up to 1° for all attitude angles in x, y, and z directions is accepted to be sufficient to provide reliable attitudes (Theil et al., 2003). The angles determined here appear to be very small to give rise to attitude angles greater than 1° . Even though difference in angles are small, for more accurate and reliable attitude predictions, the model that gives smaller angles with the observations should be preferred, under especially geomagnetically active conditions when the deviations from observations were expected to be larger.

Table 4 compares the root mean square (RMS) error between the models and the observations during the quiet day (left) and active day (right). The second and third columns in both tables are the RMS errors for the differences between the magnetic field components of the models and the observations. Namely, the differences between the IGRF and the observations and (second column) and the differences between T89 and the observations (third column). Table 4 for the active conditions on the right was performed by using the differences for the data corresponding to the part of the differences corresponding to $K_p > 4$, defined as the active times. Comparison of right and left panels shows that the RMS errors in predicting the observed magnetic field components are smaller during the magnetically quiet day as opposed to the magnetically active day. Here we see that the RMS error for the total magnetic field is the largest compared to the RMS error in the components. For the components, RMS errors are smallest for \mathbf{B}_z and largest for \mathbf{B}_y . T89 model gives much smaller RMS error than those of IGRF model in both quiet and active conditions, implying its predictions are closer to the observations. The errors during the active times increase in both models. Overall, T89 model, compared to IGRF, shows better performance in predicting both the magnetic field components and also the magnetic field strength and agrees better with the observations based on RMS errors. One point that needs emphasis from the point of satellite attitude purposes is that even during the quiet days, noticeable differences with the observations occur in predictions of both IGRF and T89 models. Differences become larger during the active days, especially in IGRF model.

The last row in Table-4 displays and quantifies differences in the angles averaged over the time intervals studied, i.e. 24 hours. We can see that the average angles from both models differ mostly during the geomagnetically active days. IGRF's angles were found to be larger than that of T89 by about 32% during the geomagnetically active times while they differ by about 4% for quiet times.

Figure 6 presents the second case and from C/NOFS angle. The quiet and active day panels are shown on the left and right respectively. Similar to previous case, K_p is 0 throughout the day in this event as well. In this case too, models give the largest difference for \mathbf{B}_x component and the smallest for the \mathbf{B}_y component. The magnitude of the differences varies from 80 nT for \mathbf{B}_x to -30 nT for \mathbf{B}_z from both models. For \mathbf{B}_y component, differences are around 10-20 nT in case of T89 and close to 0 nT for IGRF. The right panels for active day in Figure 6 display that K_p levels are around 4 and exceed 4 during the day, indicating that the geomagnetic activity increased. In these panels, we can see the differences become large as the geomagnetic activity becomes stronger. IGRF shows slightly larger differences when compared to T89. Differences with the observations during the active day vary around 100 nT for \mathbf{B}_x component in both models while differences for \mathbf{B}_y are seen to be around 30-40 nT. Differences in \mathbf{B}_z component are negative in case of IGRF and positive in T89 models indicating IGRF predictions for \mathbf{B}_z are smaller up to 40 nT and T89 models are larger up to 20 nT. Differences between the models indicate that both models B_x and B_y predictions are closer being IGRF slightly larger for \mathbf{B}_x and slightly smaller for \mathbf{B}_y . For \mathbf{B}_z , however, IGRF is considerably smaller than T89 varying from 20 nT up to a maximum of 80 nT.

Figure 7 illustrates the average angles for Case 2, January 5, 2013 and August 4, 2010. Both models give an angle on the order of 0.15° during quiet day and differ during the active day between 0.1° and 0.2°. Differences are larger during the high geomagnetic activity periods seen from 0 to 06:00 UT, and 08:00 UT to 24:00 UT. When K_p reaches 6, the differences are seen to reach a maximum of 0.2°. During this event, AE is high at the beginning but becomes lower after 12:00 UT. However, D_{st} is seen to vary from -30 nT to -80 nT indicating geomagnetic storm presence, even when AE is low. The variations in average angle is due to the geomagnetic storm as associated with a Coronal Mass Ejection (CME) in the solar wind (not given).

Table 5 gives the RMS errors for this case. As in the previous case, the largest RMS error is seen in B_{tot} , followed by \mathbf{B}_y , \mathbf{B}_x and \mathbf{B}_z respectively during both quiet and active days. The errors are larger, almost twice, during the active days and in IGRF predictions during both quiet and active times. The difference in average angles is slightly larger or equal during quiet days than active and in IGRF model than in T89 model. The range of angles is smaller than 1° in this example too.

Figure 8 illustrates the differences between the models and observations as well as between the models for SWARM A satellite during the magnetically quiet day (January 18, 2014) and active day (February 20, 2014) respectively. The panels from top to bottom are the same as in the previous figures. The magnetic field components from the satellite magnetometer and from the T89 and IGRF models were again orbit averaged using running mean procedure. The top, right panel on the left ensures that the day is quiet with K_p varying between 0 and 1. The differences between the models and the observations are seen to be less than ±10 nT in panels b and c. The close

examination of the panels shows that T89 model predicts \mathbf{B}_y component as the best in this case; this is followed by the prediction of the \mathbf{B}_z component. On the average, both of them is close to zero which means that they are equal to observed \mathbf{B}_y and \mathbf{B}_z . T89 predict the \mathbf{B}_x component as the largest which means \mathbf{B}_x deviates the most from the observed \mathbf{B}_x component. IGRF model, on the other hand, predicts the \mathbf{B}_z component the least by giving the largest deviation from the observed \mathbf{B}_z component. It is about -25nT which means that the observed \mathbf{B}_z component is larger than the IGRF predicted \mathbf{B}_z . The best predicted component by IGRF is also \mathbf{B}_y component being close to zero on the average. The differences for \mathbf{B}_x is about 13nT on the average as well. These differences are small. Panel d in Figure 8 compares the model outputs for this case by taking the difference between IGRF and T89 models respectively. It is seen that the \mathbf{B}_z component differs the most between two models. Model differences between \mathbf{B}_x and \mathbf{B}_y components vary between ± 20 nT and close to zero on the average.

The second and third panels on the right of Figure 8 demonstrate the differences between the model and the SWARM data during the geomagnetically active day. Contrary to the panels on the left, magnetic field vectors from IGRF and T89 in these panels are seen to be vary up to 100 nT during the geomagnetically active day. The first panel indicates the presence of moderate geomagnetic activity with a K_p maximum at 6 almost throughout the day. We can see that the differences with the observations in both models are large corresponding to the increased K_p . Examining T89 panel shows that B_x has a maximum difference about 100 nT while \mathbf{B}_y and \mathbf{B}_z differences are closer to zero. T89 model predicts \mathbf{B}_y and \mathbf{B}_z components the best. IGRF model, on the other hand, has larger differences compared to T89 model in all components. B_x varies up to 100 nT at the maximum, and \mathbf{B}_y and \mathbf{B}_z vary up to 25 nT and 50 nT respectively. We can see this also in panel d where the differences between two models are shown component to component. Both model differs the most in \mathbf{B}_z , \mathbf{B}_x and then \mathbf{B}_y starting at the time of the magnetic activity at about 02:00 UT.

Figure 9 gives the angle between the model and observed magnetic fields during the quiet (left) and magnetically active (right) day respectively. First two panels on the left indicate the absence of geomagnetic storm ($D_{st} > -40$ nT) and magnetospheric substorms ($AE > 100$) while the panels on the right indicate a very strong magnetospheric substorm ($AE > 100$ nT) and a strong geomagnetic storm with $D_{st} < -40$. Comparing the angles between the magnetic field vectors between the observations and the models shows that the differences are small. The differences are about 0.05° during the quiet day while it is maximum at 0.24° and 0.2° in the case of geomagnetically active day for IGRF and T89 models respectively. The magnetic field vector predicted by T89 model is closer to the observed magnetic field vector while IGRF predicts slightly larger angles. Difference in angles is larger corresponding to the increased activity period from 02:00UT to 11:00 UT when K_p is equal to 6 for 9 hours.

In Table 6, RMS errors were presented for both quiet day and active day for SWARM events. As in the previous comparisons, when we examine the magnetic field components, it is seen that the smaller RMS errors were obtained during the quiet days as compared to the active days from both models. IGRF RMS errors increases almost twice during the active times. When the models compared to each other during quiet and active days, T89 model gives smaller errors during active

times in general for all components while during the quiet times, its RMS error is larger for B_x and B_{tot} but smaller for B_y and B_z compared to that of IGRF. When we look at the average angle, we see that the angles during the active times are much larger than those of quiet times for both model predictions. Between the models, IGRF model gives larger angles for both quiet (35%) and active (3%) days than T89 model. Also, both models predict larger angles during the active times by about 60-70% than those of quiet times.

Figure 10 was produced to present a statistical result on the angles predicted by the models based on these three geomagnetically active (blue) and quiet days (orange). Upper panel in the figure illustrates the bar plot of the angles between the magnetic field vector observed by both spacecraft and their corresponding IGRF magnetic field vectors while the lower panel give the same for T89 model. We notice from the figure, for both quiet and active days, the angles are less than 0.3° which seems to be the threshold for these spacecraft for the events studied. Comparing both panels shows that angles predicted by T89 are smaller than 0.175° during both quiet and active days and there are fewer cases for angles larger than 0.15° during the active times when compared to the IGRF model. The distribution of the active time average angles for T89 model are skewed towards the lower angles than 0.15° while that for IGRF model has a skew towards larger angles than 0.15° . In the lower end side, the angles from IGRF model has more cases larger than 0.05° during the quiet days compared to T89 which presents more cases with angles less than 0.05° at these times. Overall the average angle for all cases for IGRF model is 0.126° during the quiet days while it is 0.170° during active days. The average angles for T89 model are seen to be 0.114° for the quiet days and 0.136° for the active days.

Figure 11 compares the differences in angles from two models during the active (blue) and quiet (orange) times by subtracting T89 angles from IGRF angles. The vertical axis was normalized to the total number of data in each case. Several points that the figure shows are: First, the zero degree angles indicate that the magnetic field vectors from both models are the same. Secondly, most of the differences are positive indicating that IGRF angles are larger than those of T89. Third, the negative angles, which are not the majority, show that T89 model angles are larger than those of IGRF. Considering these facts, this figure's highlights are below:

1. During both the active and quiet days, most of the angles are positive indicating that IGRF gives larger angles than T89 model does. In these cases, T89's magnetic field vectors are closer to the observed magnetic field.
2. The differences between angles from two models are larger during the active times than during the quiet times. Larger positive angles during active times shows that IGRF differs the most from T89 during the active days than quiet days.
3. Most of the time the angle between the magnetic field vectors of the models during both quiet and active times are smaller than 0.12° . The maximum is 0.033 for the quiet day and 0.011° for the active day. Most of the times, the angles can be different by about 0.01° and 0.018° for the quiet days and can often vary as 0.01° , 0.02° , 0.041° , 0.081° and 0.15° during the active days.

4. The average angle difference for the cases when IGRF angles are larger than T89 angles is 0.0128° for the quiet days and it is 0.0370° for the active days.
5. The average angle difference for the cases when T89 angles are larger than IGRF angles is 0.0026° for the quiet days and it is 0.023° for the active days.

Table-7 gives a summary of the average angles from the models compared.

4. Discussion and Summary

One of the main motivations in our paper was to determine the effects of the geomagnetic disturbances on the satellite's attitude at LEO orbits. This is related to the accuracy of the geomagnetic field predictions by the geomagnetic field models at the satellite's position. The most commonly used geomagnetic model in determining the satellite's attitude at LEO orbit is IGRF model (Babcock and Bretl, 2011; Inamori and Nakasuka, 2012). The accuracy of the IGRF-10 and IGRF-11 models were tested against data from UARS, Oersted and CHAMP spacecraft and found that the models are accurate within 1° for 92% times in upper atmosphere (Matteo and Morton, 2011). However, the authors of this paper cautioned that the variations in the magnetic field occur as a result of the geomagnetic storms and IGRF may not always be appropriate to modelling the magnetic field at LEO. Similarly, (Archer et al., 2015) used IGRF to calibrate the magnetometers on CINEMA CubeSat and found root mean squared deviations in field magnitudes from IGRF of 1.95% for the attitude mode. Such accuracy in the overall magnetic fields are found to be sufficient for attitude estimation (Natanson et al., 1990). Even though IGRF model was found to be sufficient to represent the magnetic field required for the satellite attitude, the concerns were raised as in relation to the solar activity and geomagnetic activity (Archer et al., 2015; Matteo and Morton, 2011).

In our study, we have compared two geomagnetic field models, IGRF-12 and T89, to compare both with the magnetic field predictions at LEO orbit using two spacecraft magnetometer data. We found that both models differ from the observations during the geomagnetically active times as well as during the quiet times. The differences are larger in the case of the IGRF-12 model compared to T89 models. Differences vary according to the magnetic field components. The comparisons with the data from two satellites, C/NOFS and SWARM, indicate that the largest differences were seen in B_x and B_y while the smallest differences were found in B_z component. The differences between the observed magnetic field vector and that predicted by the model were obtained larger during the high geomagnetic periods. The angle between the vector magnetic field from the satellite measurements and models were shown to be smaller in the case of the T89 model, indicating that T89 model estimates are closer to the data. The differences in magnetic field components and the vector magnetic fields were found to be larger in the case of IGRF model during both geomagnetically quiet and active times. T89 model is expected to agree better with the observations, especially during the geomagnetically active times, because it is constructed such that the model includes variations resulting from both internal sources from the Earth's dynamo and crust and also external sources such as solar wind, interplanetary magnetic field, consequently geomagnetic storms and substorms. The fact that IGRF shows larger discrepancies indicates that

for better attitude predictions during especially geomagnetically active times, external sources are needed to be taken into account.

To summarize, in this study, we compared magnetic field measurements from magnetometers onboard two different satellites at LEO orbit with those from IGRF-12 and T89 models to address on the noise referred as the angle in our study that will eventually be used to determine the satellite attitude. A follow-up study is underway how much these differences affect the attitude angles described as Euler angles. We highlight our results represented here as below:

1. In general, both models show differences with the observed magnetic fields during the geomagnetically active times as well as quiet times.
2. IGRF model gives larger differences compared to T89 during both quiet times as well as active times. Differences during active times are the largest.
3. During the geomagnetically active time, T89 model gives closer estimations to the observations.
4. The largest differences were seen in B_x in general and the smallest in B_z .
5. The differences in the strength of the magnetic field are much smaller than those of magnetic field components.
6. Differences between the models are seen the largest in B_z and smaller in B_x and B_y .
7. Large differences in the angle and in the magnetic field components correspond to large geomagnetic activity index, K_p .
8. The angle between vector magnetic field from the models and the data is obtained less than 1° for C/NOFS and SWARM data. The differences between the satellites stem from the properties of the instruments used onboard in these satellites.

These differences imply that the model estimate the magnetic field orientations at the satellite location satisfactorily so that the angle between the vector magnetic fields is small. From the satellite attitude view, this agreement is very important. Also, the RMS errors for the field components were found to be small. Although both models were seen to be appropriate for calculating the magnetic fields at the satellite position at LEO, it is clear that IGRF model gives larger differences compared to T89 model during both quiet and active times. The difference in the angle between the model and the observed magnetic field directions which is calculated less than 1° is within the acceptable range and both models can be used for attitude predictions within their error ranges. Both models have their advantages and disadvantages to be used in the attitude estimations. Since the differences are small, the attitude system controllers may continue to use IGRF instead of T89 to avoid its continues need to acquire the magnetic index data such as K_p , AE and Dst on board the satellite. This will depend on their preference. Here we demonstrated that an alternative model, physically improved, can be used during especially geomagnetically active times, for more accurate attitude estimations. Results of this study are especially important where a high accuracy is needed for attitude control at LEO and where we need to decide which geomagnetic model to use to achieve better attitude. To our knowledge, this is the first paper that studied the effects of the environment on the satellite attitude and it should be pursued with more statistical analysis with different types of satellite orbits at different altitudes, within different near

Earth space environment conditions, not just LEO but also where the magnetometers are used for detection of the satellite attitudes.

Acknowledgement

This work was supported by TUBITAK project No: 113E595. The author Demet Cilden-Guler was supported by ASELSAN and TUBITAK PhD Scholarships in some part of the time of this work. We communicated with Nikolai Tsyganenko to obtain the most updated version of his models in Matlab. We thank him for his kind advice. The spacecraft data from C/NOFS were obtained from NASA's website CDAWeb (<http://cdaweb.gsfc.nasa.gov>) and the data from SWARM were obtained from the shared ftp site from the ESA's web-site (<http://earth.esa.int/>). We thank all the data providers.

References

- Ainscough, T., Zanetti, R., Christian, J., Spanos, P.D., 2015. Q-Method Extended Kalman Filter. *J. Guid. Control. Dyn.* 38, 752–760. doi:10.2514/1.G000118
- Alonso, R., Shuster, M.D., 2002. Two Step: A Fast Robust Algorithm for Attitude-Independent Magnetometer-Bias Determination. *he J. Astronaut. Sci.* 50, 433–451.
- Alonso, R., Shuster, M.D., 2002. Attitude-Independent Magnetometer-Bias Determination: A Survey. *J. Astronaut. Sci.* 50, 453–475.
- Archer, M.O., Horbury, T.S., Brown, P., Eastwood, J.P., Oddy, T.M., Whiteside, B.J., Sample, J.G., 2015. The MAGIC of CINEMA: first in-flight science results from a miniaturised anisotropic magnetoresistive magnetometer. *Ann. Geophys* 33, 725–735. doi:10.5194/angeo-33-725-2015
- Babcock, E.P., Bretl, T., 2011. CubeSat Attitude Determination via Kalman Filtering of Magnetometer and Solar Cell Data, in: 25th Annual AIAA/USU Conference on Small Satellites.
- Communications/Navigation Outage Forecasting System (C/NOFS) [WWW Document], 2016. URL <https://directory.eoportal.org/web/eoportal/satellite-missions/content/-/article/cnofs> (accessed 8.11.16).
- Coordinated Data Analysis Web (CDAWeb) [WWW Document], 2017. URL https://cdaweb.gsfc.nasa.gov/istp_public/ (accessed 7.29.17).
- Data Analysis Center for Geomagnetism and Space Magnetism, n.d. Geomagnetic Data Service, Kyoto [WWW Document]. URL <http://wdc.kugi.kyoto-u.ac.jp/wdc/Sec3.html> (accessed 9.16.17).
- European Space Agency, 2016. Swarm (Geomagnetic LEO Constellation) [WWW Document]. URL <https://directory.eoportal.org/web/eoportal/satellite-missions/s/swarm> (accessed 8.11.16).
- Farfield, D.H., 1991. An Evaluation of the Tsyganenko Magnetic Field Model. *J. Geophys. Res.* 96.

This is an Author Accepted Manuscript version of the following article: D. Cilden-Guler, Z. Kaymaz, C. Hajiyev, Evaluation of geomagnetic field models using magnetometer measurements for satellite attitude determination system at low earth orbits: Case studies. *Advances in Space Research*, 61(1), pp. 513-529, 2018. The final authenticated version is available online at: <https://doi.org/10.1016/j.asr.2017.10.041>

Finlay, C.C., Olsen, N., Kotsiaros, S., Gillet, N., Tøffner-Clausen, L., 2016. The CHAOS-6 Geomagnetic Field Model [WWW Document]. URL <http://www.spacecenter.dk/files/magnetic-models/CHAOS-6/> (accessed 3.9.17).

Gonzalez, W.D., Joselyn, J.A., Kamide, Y., Kroehl, H.W., Rostoker, G., Tsurutani, B.T., Vasyliunas, V.M., 1994. What is a geomagnetic storm? *J. Geophys. Res.* 99, 5771. doi:10.1029/93JA02867

Hajiyev, C., Bahar, M., 2003. Attitude Determination and Control System Design of the ITU-UUBF LEO1 Satellite. *Acta Astronaut.* 52, 493–499.

Hajiyev, C., Cilden Guler, D., 2017. Review on gyroless attitude determination methods for small satellites. *Prog. Aerosp. Sci.* 90, 54–66. doi:10.1016/j.paerosci.2017.03.003

Hapgood, M.A., 1992. SPACE PHYSICS COORDINATE TRANSFORMATIONS : A USER GUIDE. *Plan. Sp. Sci* 40, 71–717.

Inamori, T., Nakasuka, S., 2012. Application of Magnetic Sensors to Nano and Micro-Satellite Attitude Control Systems, in: *Magnetic Sensors - Principles and Applications*. InTech. doi:10.5772/34307

Krebs, G.D., 2016. C/NOFS (Communications / Navigation Outage Forecasting System) [WWW Document]. URL http://space.skyrocket.de/doc_sdat/cnofs.htm (accessed 8.11.16).

Lichten, S.M., 2008. Cutting Edge GPS Science Applications.

Loewe, C.A., Prölss, G.W., 1997. Classification and mean behavior of magnetic storms. *J. Geophys. Res. Sp. Phys.* 102, 14209–14213. doi:10.1029/96JA04020

Lowes, F.J., 2014. An estimate of the errors of the IGRF/DGRF fields 1945–2000. *Earth, Planets Sp.* doi:10.1186/BF03352353

Matteo, N.A., Morton, Y.T., 2011. Ionosphere Geomagnetic Field: Comparison of IGRF Model Prediction and Satellite Measurements 1991–2010. *Radio Sci.* 46. doi:10.1029/2010RS004529

Maus, S., Manoj, C., Rauberg, J., Michaelis, I., Lühr, H., 2010. NOAA/NGDC candidate models for the 11th generation International Geomagnetic Reference Field and the concurrent release of the 6th generation Pomme magnetic model. *Earth Planets Space*, 62, 729–735. doi:10.5047/eps.2010.07.006

Natanson, G.A., McLaughlin, S.F., Nicklas, R.C., 1990. A method of determining attitude from magnetometer data only, in: *Flight Mechanics(Estimation Theory Symposium*. NASA, Goddard Space Flight Center, US, MD, United States, pp. 359–378.

NOAA, 2011. NOAA Space Weather Scales [WWW Document]. URL <http://www.swpc.noaa.gov/noaa-scales-explanation> (accessed 7.29.17).

Olsen, N., Lühr, H., Sabaka, T.J., Mandea, M., Rother, M., Tøffner-Clausen, L., Choi, S., 2006. CHAOS—a model of the Earth’s magnetic field derived from CHAMP, Ørsted, and SAC-C magnetic satellite data. *Geophys. J. Int.* 166, 67–75. doi:10.1111/j.1365-246X.2006.02959.x

- Peredo, M., Stern, D.P., Tsyganenko, N.A., 1993. Are existing magnetospheric models excessively stretched? . *J. Geophys. Res.* 98, 15,315-343,354.
- Pfaff, R., n.d. Description of the Vector Electric Field Instrument (VEFI) on the C/NOFS Satellite [WWW Document]. URL https://vefi.gsfc.nasa.gov/vefi/Resources/VEFI_DescriptionREV.pdf (accessed 9.16.17).
- Pfaff, R., Rowland, D., Freudenreich, H., Bromund, K., Le, G., Acuña, M., Klenzing, J., Liebrecht, C., Martin, S., Burke, W.J., Maynard, N.C., Hunton, D.E., Roddy, P.A., Ballenthin, J.O., Wilson, G.R., 2010. Observations of DC electric fields in the low-latitude ionosphere and their variations with local time, longitude, and plasma density during extreme solar minimum. *J. Geophys. Res. Sp. Phys.* 115, n/a-n/a. doi:10.1029/2010JA016023
- Russel, C.T., 1971. Geophysical Coordinate Transformations. *Cosm. Electrodyn.* 2, 184–196.
- Swarm Data Access - FTP [WWW Document], 2017. URL <ftp://swarm-diss.eo.esa.int/> (accessed 7.29.17).
- Thébault, E., Finlay, C.C., Beggan, C.D., Alken, P., Al., E., 2015. International Geomagnetic Reference Field: the 12th generation. *Earth, Planets Sp.* 67, 79. doi:10.1186/s40623-015-0228-9
- Theil, S., Appel, P., Schleicher, A., 2003. Low Cost, Good Accuracy - Attitude Determination Using Magnetometer and Simple Sun Sensor, in: 17th Annual AIAA/USU Conference on Small Satellites.
- Tsyganenko, N.A., 2008. Modeling the Earth's Magnetosphere Using Spacecraft Magnetometer Data [WWW Document]. URL <http://geo.phys.spu.ru/~tsyganenko/modeling.html>
- Tsyganenko, N.A., 1995. Modeling the Earth's Magnetospheric Magnetic Field Confined within a Realistic Magnetopause. *J. Geophys. Res.* 100, 5599–5612.
- Tsyganenko, N.A., 1989. A Magnetospheric Magnetic Field Model with a Warped Tail Current Sheet. *Planet. Sp. Sci.* 37, 5.
- Vinther, K., Jensen, K.F., Larsen, J.A., Wisniewski, R., 2011. Inexpensive Cubesat Attitude Estimation Using Quaternions And Unscented Kalman Filtering. *Autom. Control Aerosp.* 4.

Tables

Table 1. Orbital properties of the spacecraft used in this study.

Satellite	C/NOFS	SWARM A
Operation Time	April 16, 2008 Nov 28, 2015	Nov 22, 2013- Present
Orbit	Elliptical	Near-polar, circular
Eccentricity	0.032	0.0003099
Inclination (deg)	13	87.4
Apogee	853	466
Perigee	405	485
Altitude Range (km)	390-736	466-485
Period (min)	97.3	91
Magnetometer Type	Fluxgate	Fluxgate

Table 2. Magnetically quiet and active days selected for the study.

Case No	Satellite	Quiet days	Active Days
Case 1	C/NOFS	7 March 2009	17 March 2013
Case 2	C/NOFS	5 January 2013	04 August 2010
Case 3	SWARM A	18 January 2014	20 February 2014

Table 3. Classification of geomagnetic storm and substorms based on D_{st} , K_p , and AE magnetic indices (Loewe and Prölss, 1997; NOAA, 2011).

Magnetic Index	No-to-Weak Storm/Substorm	Moderate Storm/Substorm	Strong Storm/Substorm
K_p	<4	4-6	>6
D_{st}	>(-40)	(-40)-(-100)	<(-100)
AE	<100	100-1000	>1000

Table 4. RMS errors for C/NOFS (Case-1) comparisons for geomagnetically quiet day (left) and active day (right).

07 March 2009 (Quiet Day)		C/NOFS		17 March 2013 (Active Day)		C/NOFS	
RMS Error		IGRF	T89	RMS Error		IGRF	T89
Bx (nT)	64.9	69.5		Bx (nT)	74.43	69.70	
By (nT)	36.9	34.6		By (nT)	104.42	105.92	
Bz (nT)	20.8	2.1		Bz (nT)	25.12	4.80	
Btot (nT)	79.3	79.4		Btot (nT)	120.78	117.82	
Mean				Mean			
Angle (deg)	0.1559	0.1499		Angle (deg)	0.1972	0.1335	

Table 5. RMS errors for C/NOFS (Case-2) comparisons for geomagnetically quiet day (left) and active day (right).

5 January 2013 (Quiet Day)		C/NOFS		4 August 2010 (Active Day)		C/NOFS	
RMS Error		IGRF	T89	RMS Error		IGRF	T89
Bx (nT)	37.2	33.2		Bx (nT)	113.5	102.5	
By (nT)	41.2	38.8		By (nT)	18.3	18.9	
Bz (nT)	34.1	11.0		Bz (nT)	41.3	15.1	
Btot (nT)	80.6	74.8		Btot (nT)	153.3	141.1	
Mean				Mean			
Angle (deg)	0.1645	0.1545		Angle (deg)	0.1680	0.1406	

Table 6. RMS errors for SWARM A (Case-3) comparisons for geomagnetically quiet day (left) and active day (right).

18 January 2014 (Quiet Day)		SWARM A		20 February 2014 (Active Day)		SWARM A	
RMS Error		IGRF	T89	RMS Error		IGRF	T89
Bx (nT)	25.8	27.3		Bx (nT)	44.2	45.2	
By (nT)	7.1	5.7		By (nT)	15.0	1.4	
Bz (nT)	18.6	4.7		Bz (nT)	12.1	8.1	
Btot (nT)	9.1	11.4		Btot (nT)	22.5	15.0	
Mean				Mean			
Angle (deg)	0.058	0.038		Angle (deg)	0.1376	0.1342	

Table 7. Overall evaluation of average angles.

Case No	Satellite	Quiet Day average (degree)		Active Day average (degree)	
		IGRF	T89	IGRF	T89
Case-1	C/NOFS	0.156	0.150	0.197	0.134
Case-2	C/NOFS	0.165	0.155	0.168	0.141
Case-3	SWARM A	0.058	0.038	0.138	0.134

Figures

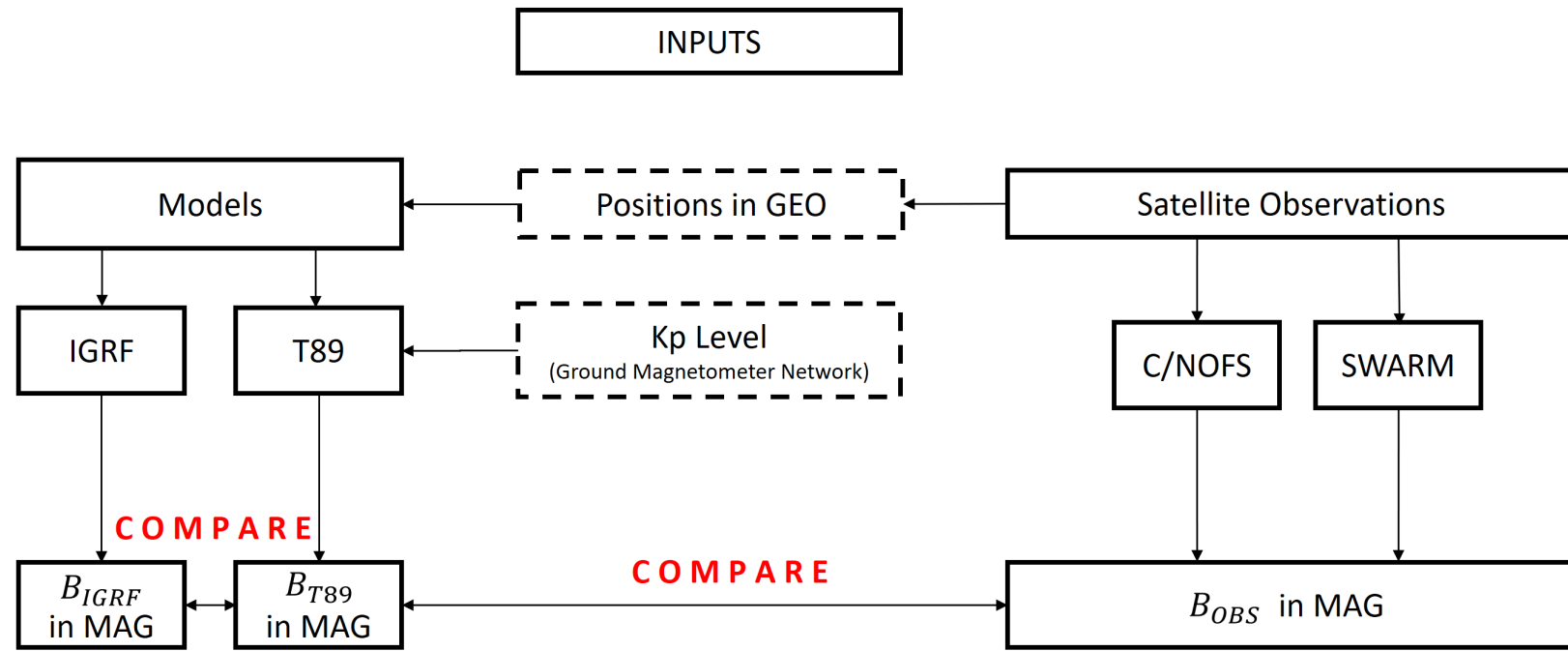


Figure 1. Flow chart for the comparisons.

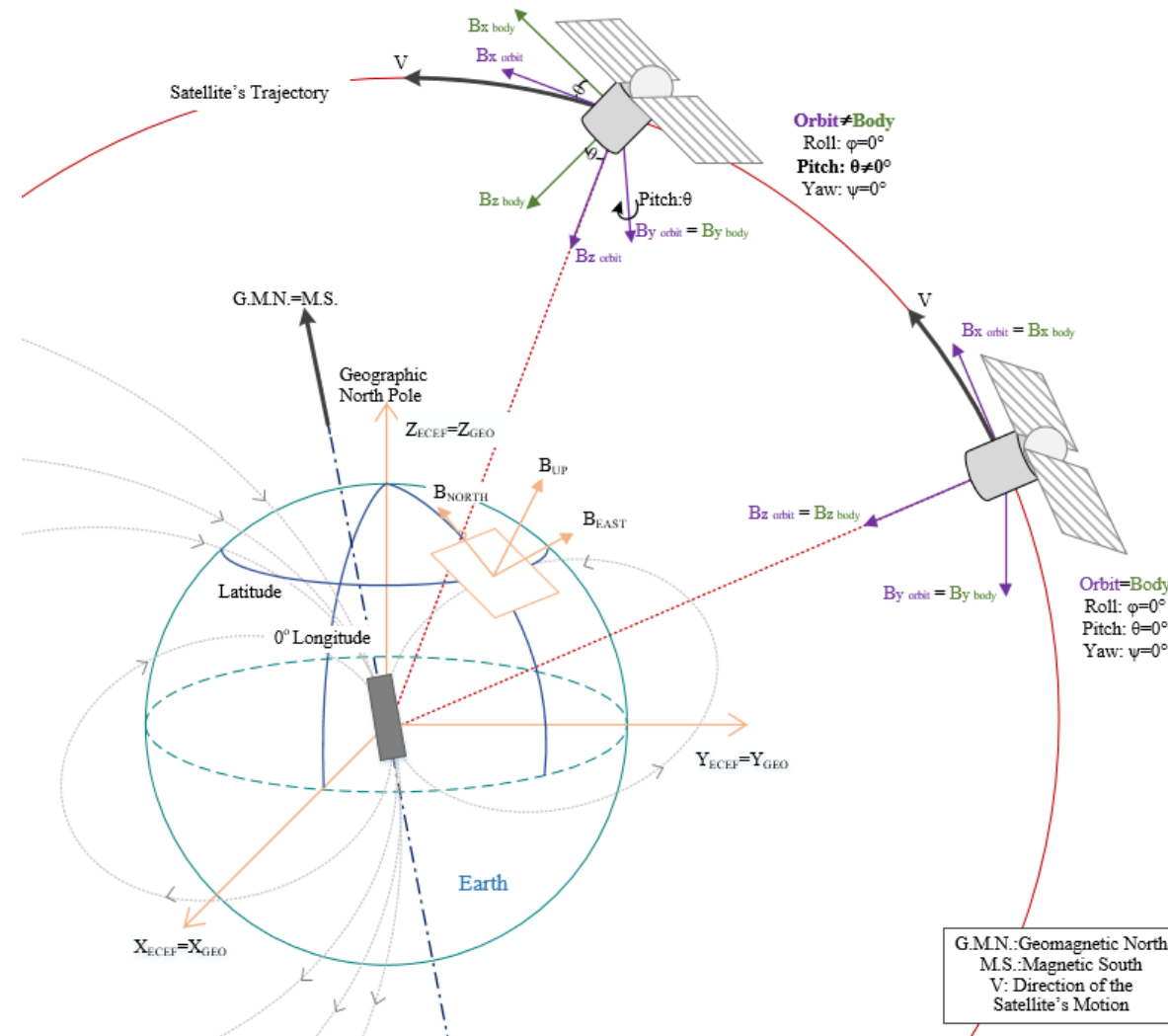


Figure 2. A sketch showing the coordinate systems along with a circular trajectory of a satellite.

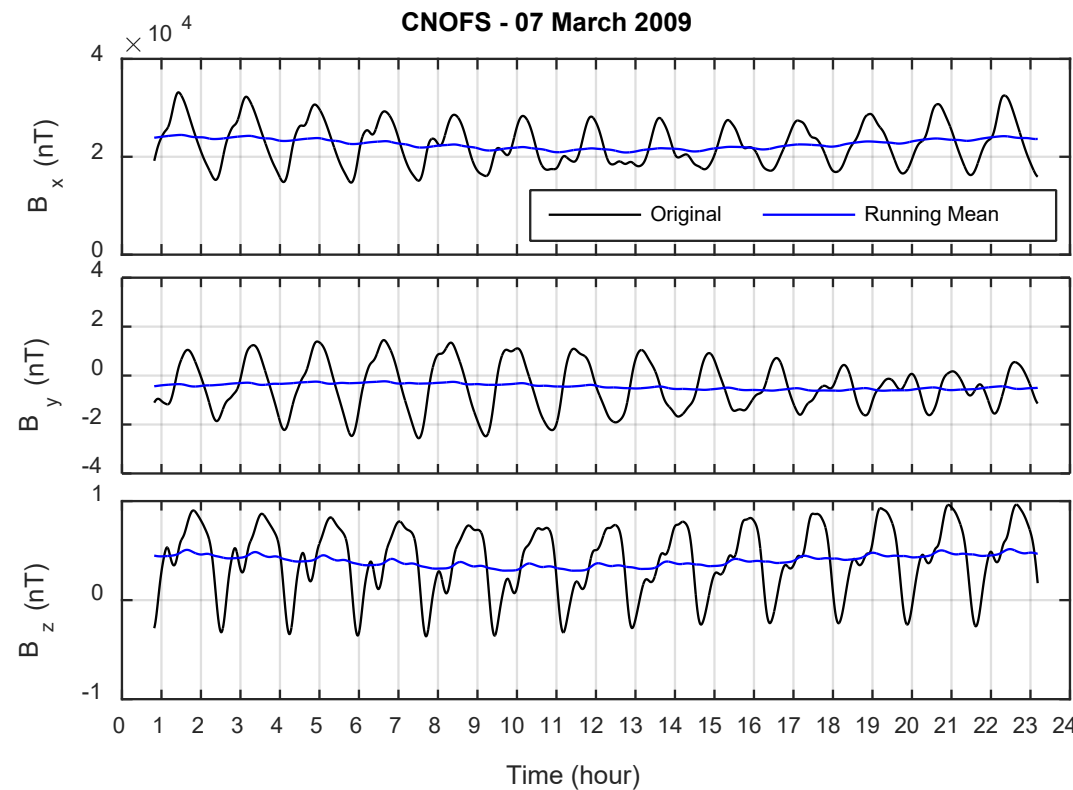


Figure 3. An example of orbit averaged data. C/NOFS magnetic field components on March 7, 2009. Black line is the original data while blue line is the orbit averaged data.

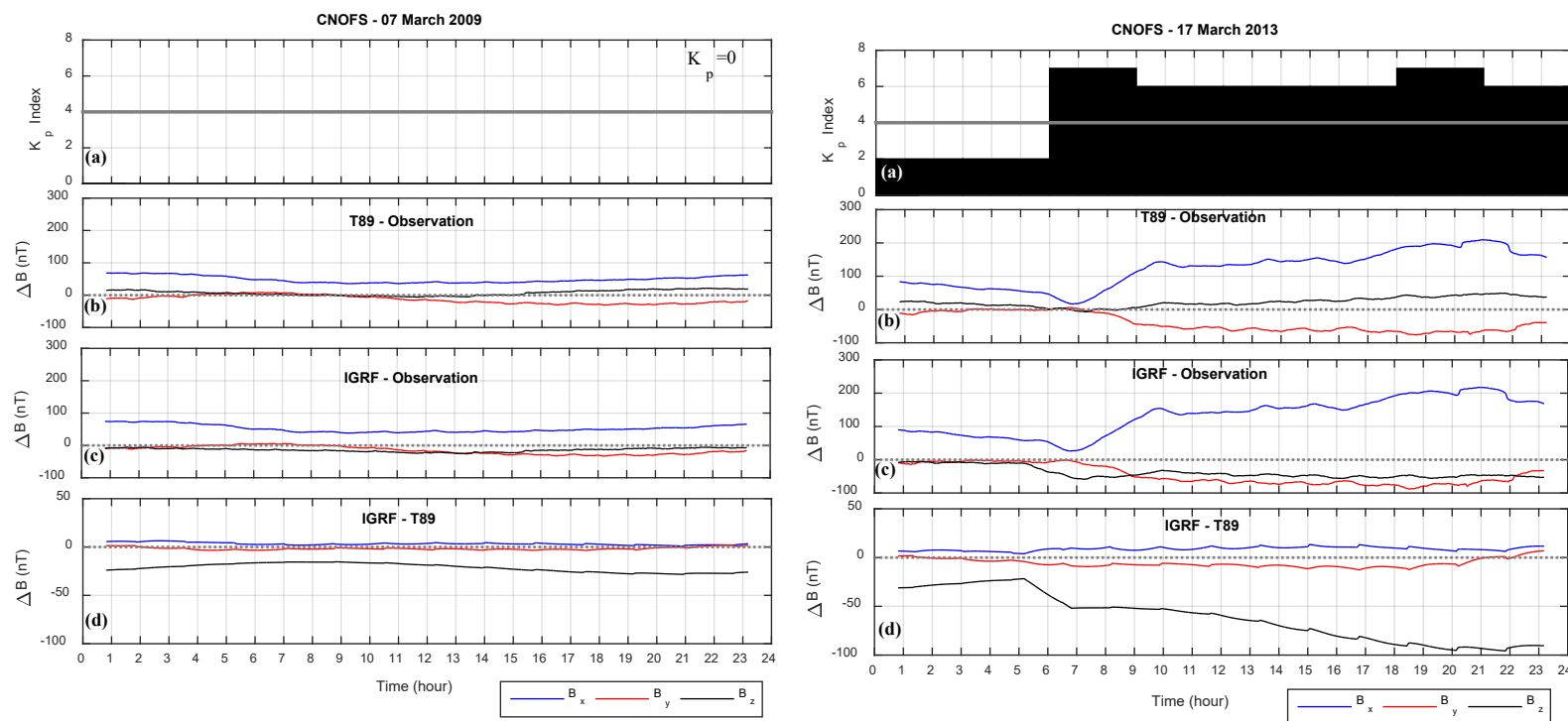


Figure 4. Differences between the observations and the model results for magnetic field components from C/NOFS satellite on March 7, 2009 when there is no geomagnetic activity (left); and on March 17, 2013 when there is geomagnetic storm (right).

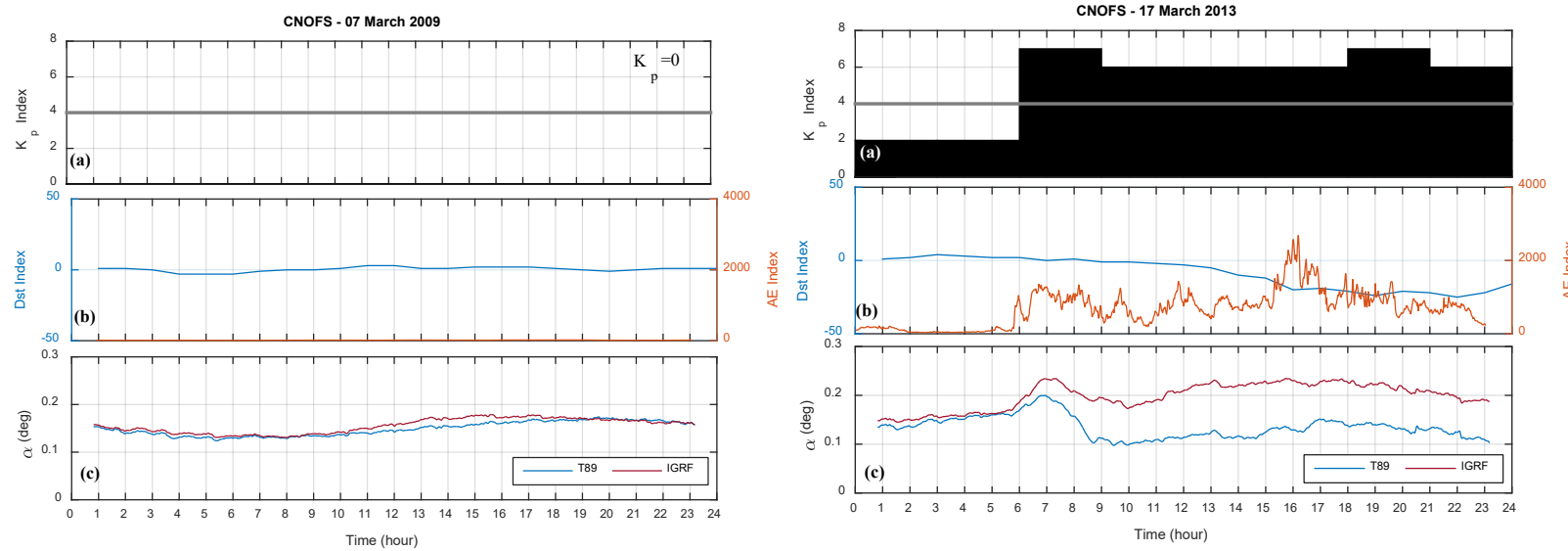


Figure 5. Angles, between the vector magnetic fields from the models and the observations, for C/NOFS satellite on March 7, 2009 when there is no geomagnetic activity (left); and on March 17, 2013 when there is geomagnetic storm (right).

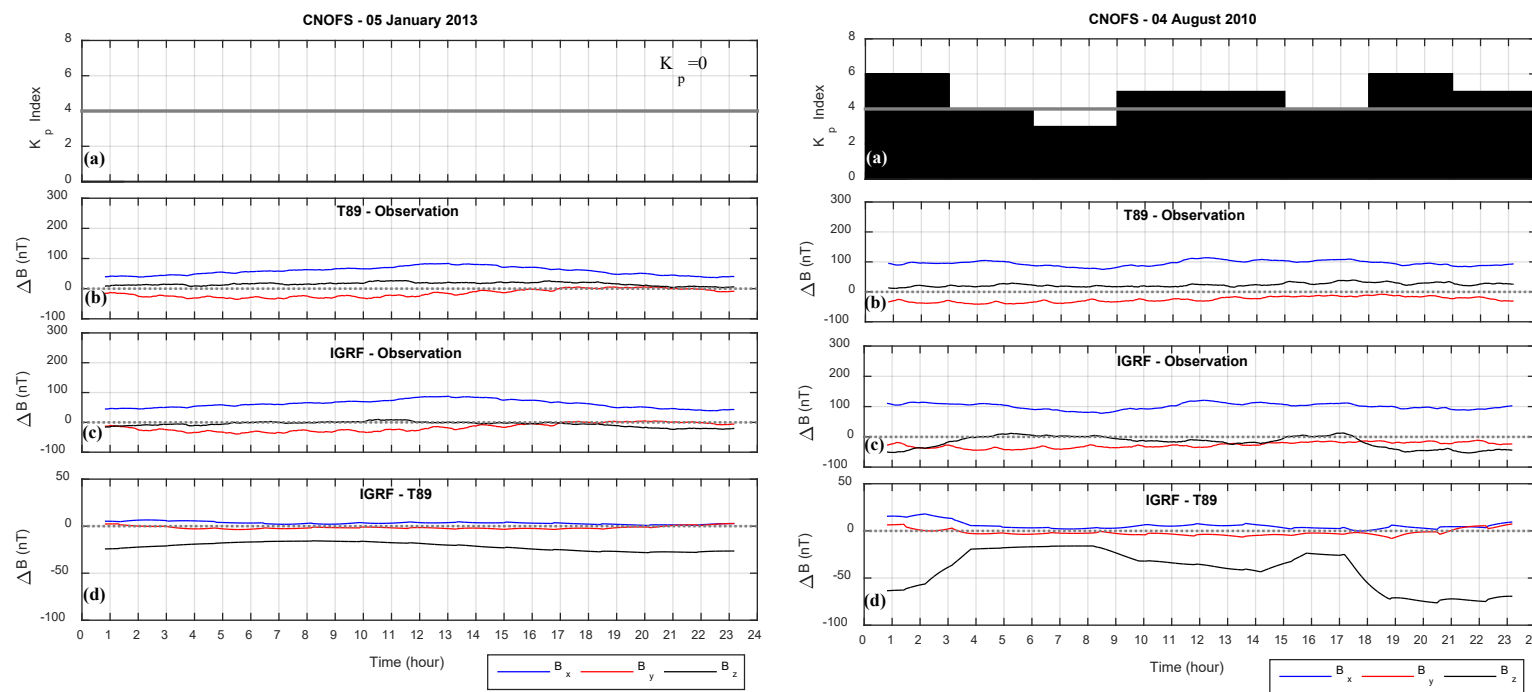


Figure 6. Differences between the observations and the model results for magnetic field components from C/NOFS satellite on January 5, 2013 when there is no geomagnetic activity (left); and on August 4, 2010 when there is geomagnetic storm (right).

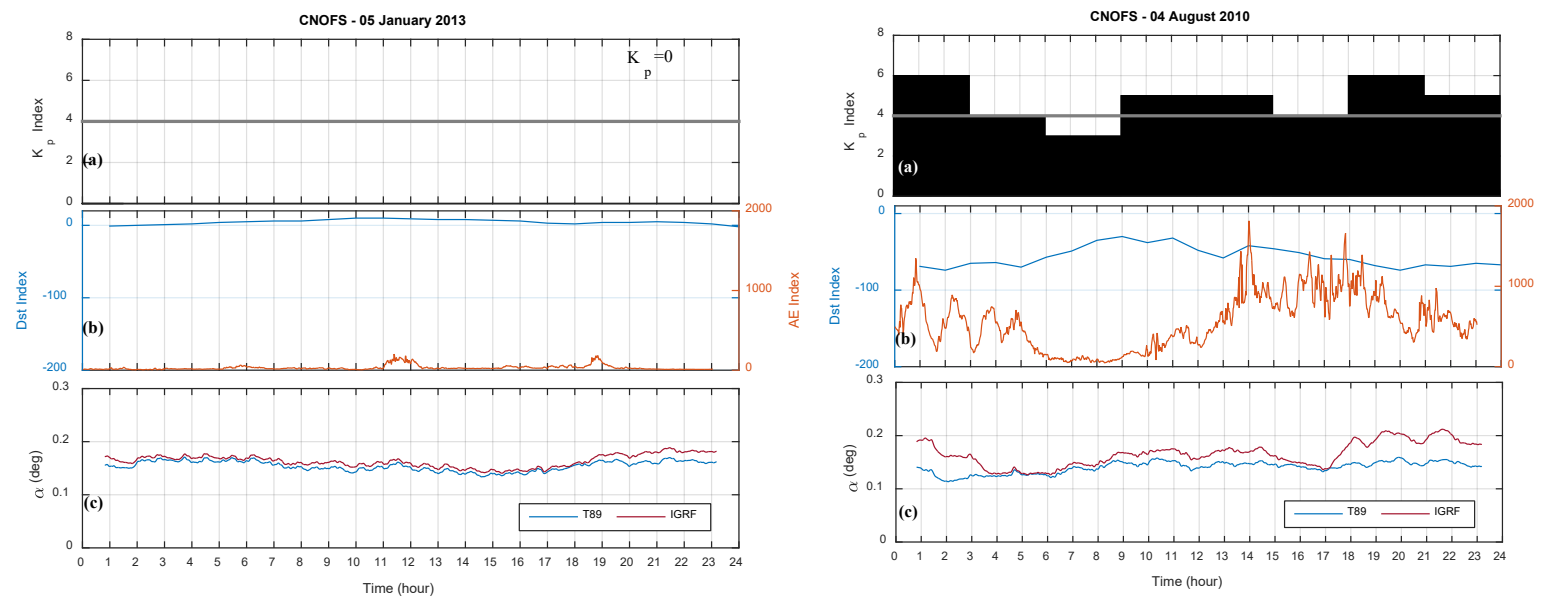


Figure 7. Angles, between the vector magnetic fields from the models and the observations, for C/NOFS satellite on January 5, 2013 when there is no geomagnetic activity (left); and on August 4, 2010 when there is geomagnetic storm (right).

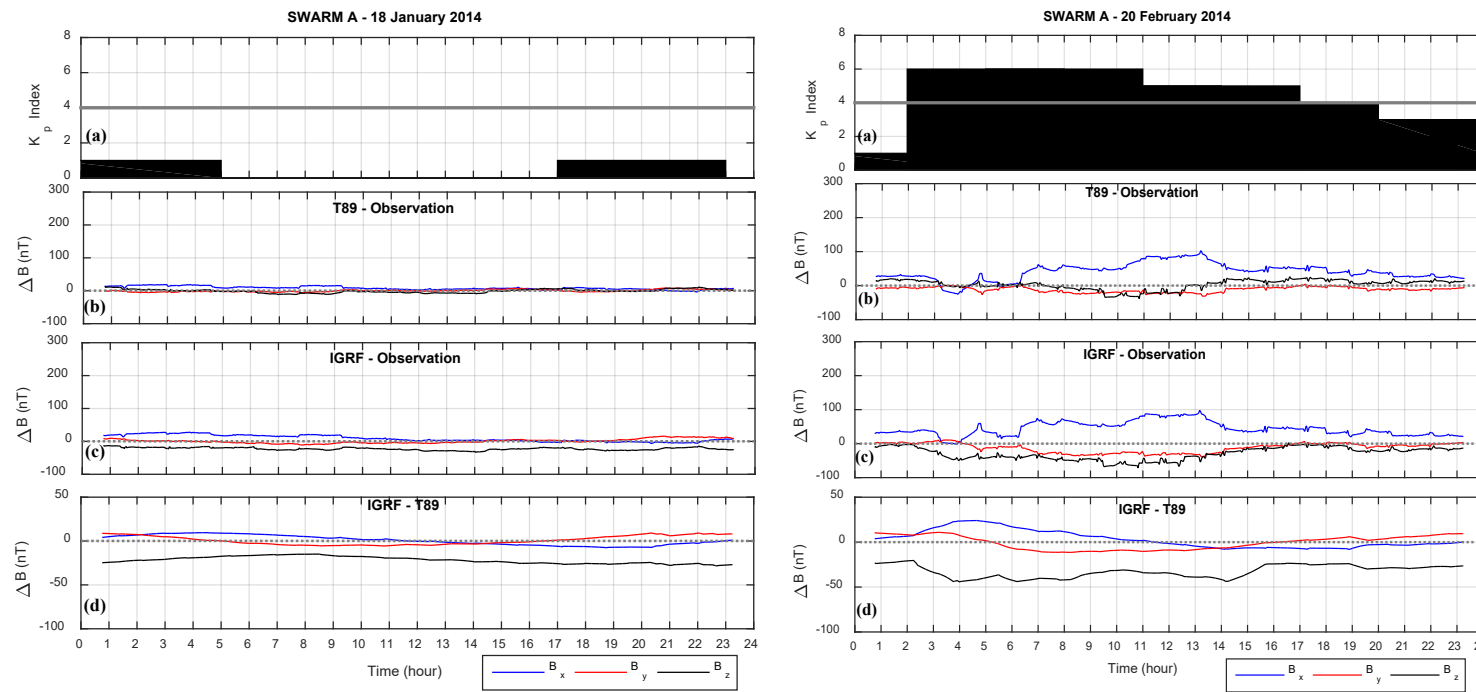


Figure 8. Differences between the observations and the model results for magnetic field components from SWARM A satellite on January 18, 2014 when there is no geomagnetic activity (left); and on February 20, 2014 when there is geomagnetic storm (right).

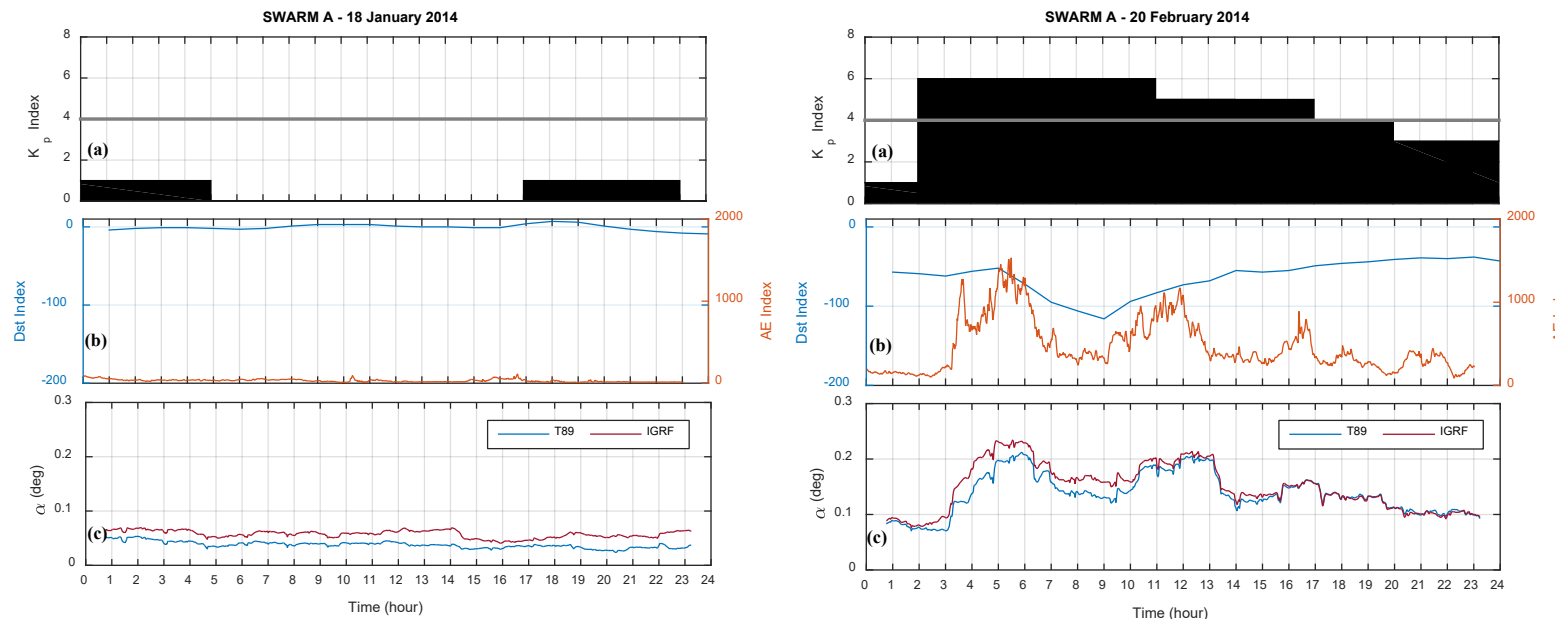


Figure 9. Angles, between the vector magnetic fields from the models and the observations, for SWARM A satellite on January 18, 2014 when there is no geomagnetic activity (left); and on February 20, 2014 when there is geomagnetic storm (right).

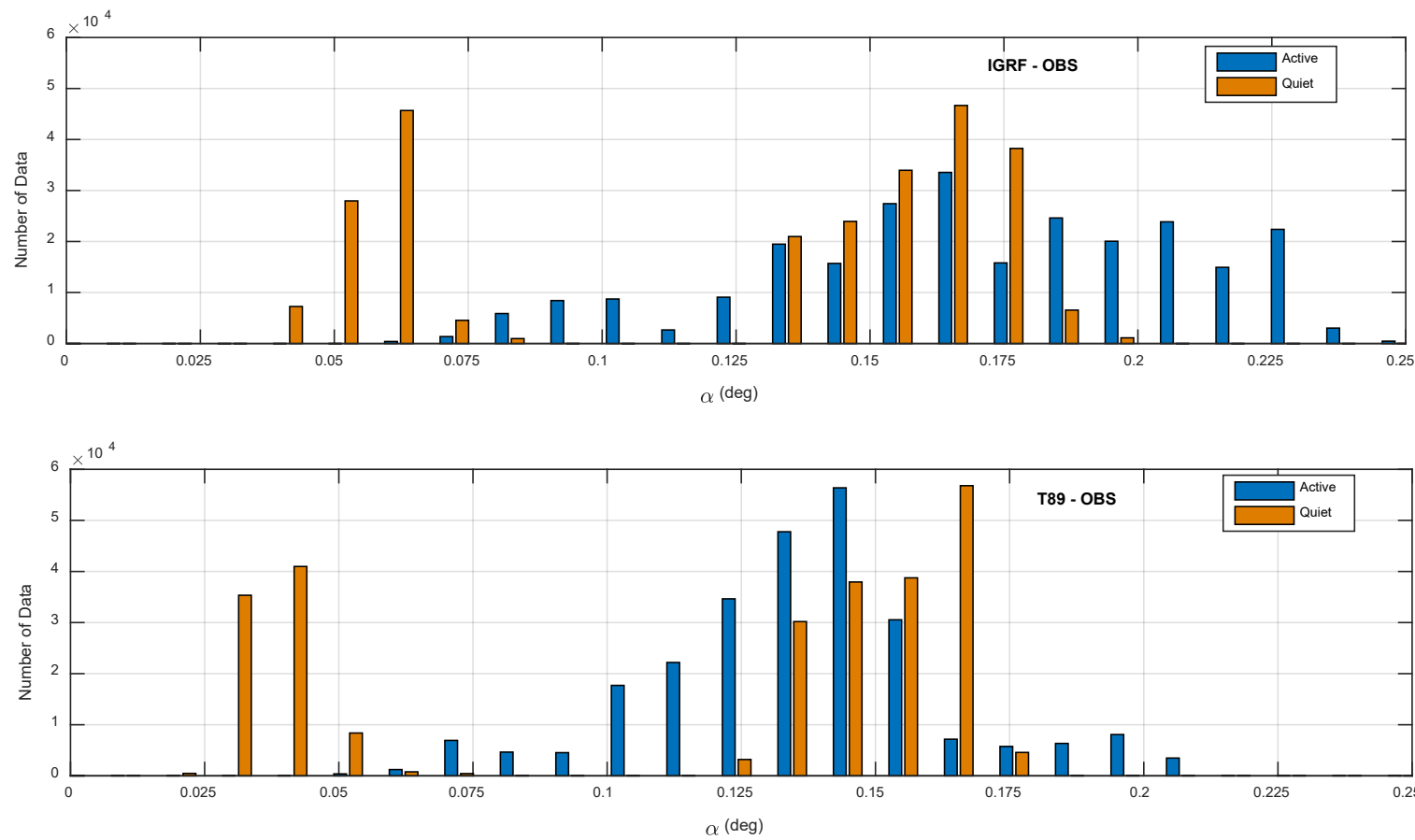


Figure 10. Angle distributions for all cases for quiet (orange) and active (blue) cases. Upper panel is for the differences between IGRF model and observations while bottom panels are for the differences between T89 model and observations.

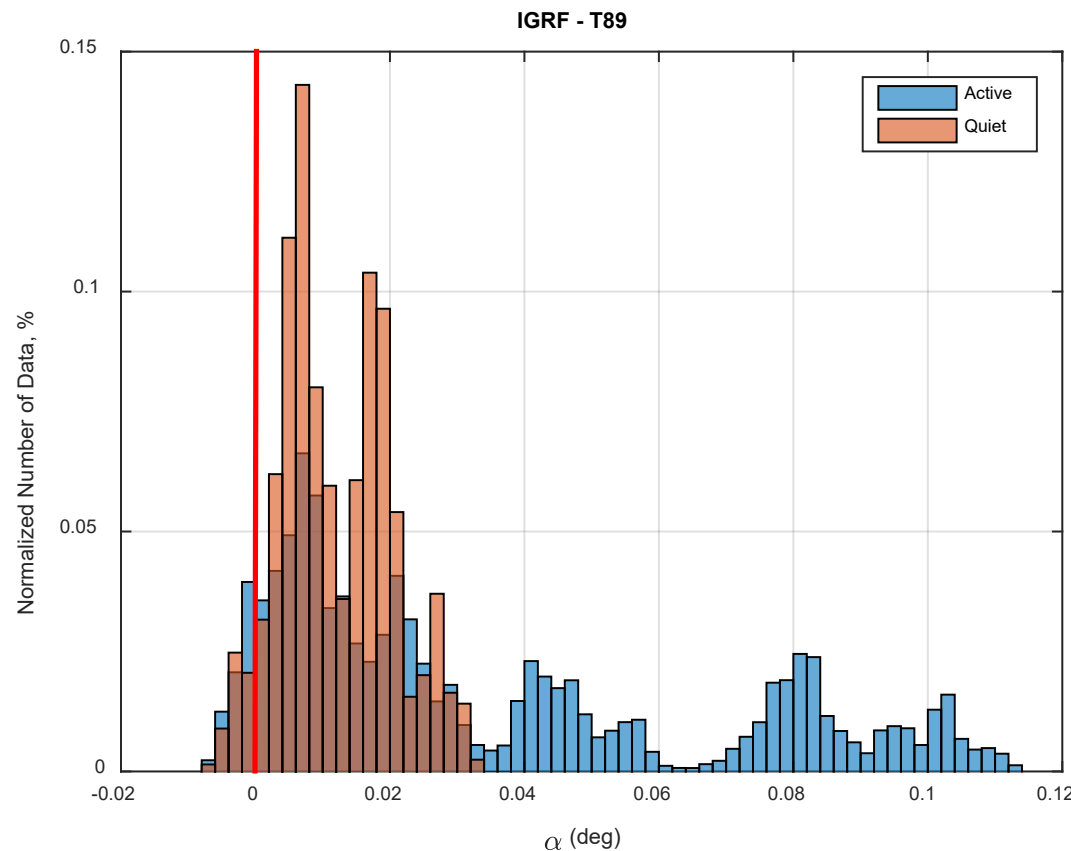


Figure 11. Comparison of difference in angles from the models: Blue is for active day and orange for quiet days.

Table Captions

Table 1. Orbital properties of the spacecraft used in this study.

Table 2. Magnetically quiet and active days selected for the study.

Table 3. Classification of geomagnetic storm and substorms based on Dst, Kp, and AE magnetic indices (Loewe and Prölss, 1997; NOAA, 2011).

Table 4. RMS errors for C/NOFS (Case-1) comparisons for geomagnetically quiet day (left) and active day (right).

Table 5. RMS errors for C/NOFS (Case-2) comparisons for geomagnetically quiet day (left) and active day (right).

Table 6. RMS errors for SWARM A (Case-3) comparisons for geomagnetically quiet day (left) and active day (right).

Table 7. Overall evaluation of the average angles.

Figure Captions

Figure 1. Flow chart for the comparisons.

Figure 2. A sketch showing the coordinate systems along with a circular trajectory of a satellite.

Figure 3. An example of orbit averaged data. C/NOFS magnetic field components on March 7, 2009. Black line is the original data while blue line is the orbit averaged data.

Figure 4. Differences between the observations and the model results for magnetic field components from C/NOFS satellite on March 7, 2009 when there is no geomagnetic activity (left); and on March 17, 2013 when there is geomagnetic storm (right).

Figure 5. Angles, between the vector magnetic fields from the models and the observations, for C/NOFS satellite on March 7, 2009 when there is no geomagnetic activity (left); and on March 17, 2013 when there is geomagnetic storm (right).

Figure 6. Differences between the observations and the model results for magnetic field components from C/NOFS satellite on January 5, 2013 when there is no geomagnetic activity (left); and on August 4, 2010 when there is geomagnetic storm (right).

Figure 7. Angles, between the vector magnetic fields from the models and the observations, for C/NOFS satellite on January 5, 2013 when there is no geomagnetic activity (left); and on August 4, 2010 when there is geomagnetic storm (right).

Figure 8. Differences between the observations and the model results for magnetic field components from SWARM A satellite on January 18, 2014 when there is no geomagnetic activity (left); and on February 20, 2014 when there is geomagnetic storm (right).

Figure 9. Angles, between the vector magnetic fields from the models and the observations, for SWARM A satellite on January 18, 2014 when there is no geomagnetic activity (left); and on February 20, 2014 when there is geomagnetic storm (right).

Figure 10. Angle distributions for all cases for quiet (orange) and active (blue) cases. Upper panel is for the differences between IGRF model and observations while bottom panels are for the differences between T89 model and observations.

Figure 11. Comparison of the difference in angles from the models: Blue is for active day and orange for quiet days.